

A neutrino flare associated with X-ray emission from TDE ATLAS17jrp

RONG-LAN LI (李荣岚)^{1,2}, CHENGCHAO YUAN (袁成超)³, HAO-NING HE (贺昊宁)^{1,2}, YUN WANG,¹
BEN-YANG ZHU (朱本阳)^{1,2}, YUN-FENG LIANG (梁云峰)⁴, NING JIANG (蒋凝)^{5,2} AND DA-MING WEI (韦大明)^{1,2}

¹Key Laboratory of Dark Matter and Space Astronomy,

Purple Mountain Observatory, Chinese Academy of Sciences, Nanjing 210023, China

²School of Astronomy and Space Sciences, University of Science and Technology of China, Hefei, 230026, Peoples Republic of China

³Deutsches Elektronen-Synchrotron DESY, Platanenallee 6, 15738 Zeuthen, Germany

⁴Laboratory for Relativistic Astrophysics, Department of Physics, Guangxi University, Nanning 530004, China

⁵CAS Key laboratory for Research in Galaxies and Cosmology, Department of Astronomy, University of Science and Technology of China, Hefei, 230026, Peoples Republic of China

ABSTRACT

Tidal disruption events (TDEs), where stars are captured or tidally disrupted by supermassive black holes, are potential sources of high-energy neutrinos. We report the discovery of a potential neutrino flare that is spatially and temporally associated with X-ray emission from TDE ATLAS17jrp. The best-fit spectrum of the neutrino flare follows a power-law with an index of $\gamma = 2.7 \pm 0.4$ and a flux normalization of $\Phi_0 = 1.7^{+6.3}_{-1.5} \times 10^{-18} \text{ GeV}^{-1} \text{ cm}^{-2} \text{ s}^{-1}$ at 100 TeV based on an analysis of 10-year track data from IceCube, and the flare duration is 61 days. We calculate that the probability of this association occurring by chance is 0.17%. Therefore, ATLAS17jrp is the second TDE (not including candidates) associated with high-energy neutrinos, following TDE AT2019dsg associated with an IceCube neutrino alert. This association can be attributed to the interaction of X-ray photons produced by the hot corona with high-energy particles accelerated by disk winds or outflows, resulting in the production of neutrinos.

Keywords: Neutrino astronomy; Time domain astronomy; Tidal disruption

1. INTRODUCTION

IceCube first detected astrophysical neutrinos in the TeV-PeV energy range in 2013, opening a new window for astrophysics and particle physics (Aartsen et al. 2013, 2014). Neutrinos interact weakly with matter and magnetic fields during their journey to Earth, offering crucial insights into the extreme environments of their cosmic sources (Abbasi et al. 2023). This characteristic highlights the importance of neutrinos in demonstrating the feasibility of multi-messenger astrophysics for pinpointing the origins of cosmic rays (Ahlers & Halzen 2017; Guépin et al. 2022; Murase & Bartos 2019). High-energy astrophysical neutrinos are primarily produced through hadronic processes via the interaction between the accelerated protons and dense matter or γ -rays in the source or in the surround environment, and prob-

ably further produce secondary particles and photons. Therefore, identifying the association between electromagnetic counterparts and neutrinos is an effective approach to tracing origins of astrophysical neutrinos.

Electromagnetic follow-up observations of IceCube real-time neutrino alerts have identified several candidate sources, which exhibit spatial and temporal associations with high-energy neutrino events. TDE AT2019dsg, TDE candidate AT2019fdr and AT2019aalc have been identified as temporally and spatially coincident with high-energy neutrinos IC191001A (Stein et al. 2021), IC200530A (Reusch et al. 2022a), and IC191119A (van Velzen et al. 2024), respectively, via the follow-up observations by the Zwicky Transient Facility (ZTF, Bellm et al. 2019). Recently, Yuan et al. (2024a) revealed that the super-bright TDE candidate AT2021lwx, similar to these three neutrino emitting TDEs, may have a delayed neutrino counterpart. Furthermore, Jiang et al. (2023) reported two cases of associations between neutrino alerts and TDE candidates from the sample of

mid-infrared outbursts in nearby galaxies (MIRONG). These investigations suggest that TDEs are likely to be an important class of neutrino sources.

TDEs are among the brightest transients in the optical, ultraviolet, and X-ray wavelengths, lasting from several months to years. They occur when a star comes close to a supermassive black hole and is disrupted by tidal forces (Rees 1988; Phinney 1989; Evans & Kochanek 1989; Cannizzo et al. 1990). Typical features proposed in TDE models include accretion disks (Hayasaki & Yamazaki 2019), coronae (Reusch et al. 2022b), sub-relativistic outflows or winds (Fang et al. 2020), and potentially jets and dust tours (Wang et al. 2011; Wang & Liu 2016; Dai & Fang 2017; Lunardini & Winter 2017; Dai et al. 2018; Zheng et al. 2023; Yuan et al. 2024b). High-energy astrophysical neutrinos are typically produced by accelerated cosmic rays interacting with target photons or dense matters. In the TDE, high energy cosmic rays can be accelerated in coronae, jets, disks, and winds (Murase et al. 2020b), and produce high energy neutrinos via interacting with thermal optical-ultraviolet (OUV), infrared (IR), X-ray photons or the surrounding matters. Winter & Lunardini (2023a) presented time-dependent interpretations for the three TDEs associated with alert events discovered by ZTF, and proposed three models in which X-ray, OUV, and IR photons serve as target photons for hadronic processes. Subsequent multi-messenger diagnoses, taking into account the accompanying electromagnetic emissions, indicate the consistency of this model with the X-ray and γ -ray constraints (Yuan & Winter 2023). Notably, delayed IR emissions from dust echos and prolonged $p\gamma$ interaction times in the region near the dust torus naturally explain the time delay between the neutrino arrival time and the optical peak of the TDE light curve.

ATLAS17jrp (Wang et al. 2022; Onori et al. 2022) is a TDE, exhibiting exceptionally bright emissions across OUV, X-ray, and IR wavelengths. Most optical-selected TDEs are weak in the infrared (Jiang et al. 2021a), while most infrared-selected candidates are optically faint (Jiang et al. 2021b), and optical-selected TDEs often lack bright X-ray emissions (Guolo et al. 2024). In contrast, ATLAS17jrp stands out due to its multi-wavelength brightness, providing a uniquely clean and comprehensive dataset for the study of TDEs and neutrino physics. In this work, we utilize time-dependent analysis to identify the neutrino flare signal associated with the electromagnetic emission from TDE ATLAS17jrp. Using 10-year muon-track data released by IceCube (Abbasi et al. 2021), we identify a neutrino flare that is spatially and temporally coincident with

the X-ray emission from TDE ATLAS17jrp. In Section 2, we introduce the observation data for ATLAS17jrp and the muon-track data from IceCube. In Section 3, we present a time-dependent analysis method for the search of neutrino flares and the searching result. In Section 4, we provide a multi-messenger model to fit the neutrino spectrum and multi-wavelength observations. We discuss the implication of our results in Section 5.

2. DATA

2.1. ATLAS17jrp

ATLAS17jrp is a TDE in the star-forming galaxy SDSS J1620+2407 at redshift 0.0655 (Wang et al. 2022), the mass of the central black hole is estimated to be $10^{6.67} M_{\odot}$ by the scaling relation between the black hole mass and stellar velocity dispersion (Jiang et al. 2021b). The event was first detected on August 3, 2017, by the Asteroid Terrestrial-impact Last Alert System (ATLAS, Tonry et al. 2018). About one month later, the flux in the ATLAS o -band peaked at MJD 57995 and then gradually declined to a quiescent state over the next 200 days, consistent with the typical $t^{-5/3}$ decline in the optical/UV light curves of TDEs. ATLAS17jrp was included in the MIRONG sample (Jiang et al. 2021b) based on the mid-infrared (MIR) flare observed by the Wide-field Infrared Survey Explorer (WISE, Wright et al. 2010). ATLAS17jrp's high MIR luminosity ($\sim 2 \times 10^{43} \text{ erg s}^{-1}$) indicates that it has a distinctive dust environment (Wang et al. 2022). *Swift*-XRT has observed the source on 19 occasions. In the first six observations, no X-ray photons were detected. From the 7th to 16th observations, soft X-ray photons were continuously detected. In the final three observations, X-ray photons were once again absent. During the 9th observation (MJD=58168.659), 19 soft X-ray photons were detected, corresponding to a peak luminosity of $1.27 \times 10^{43} \text{ erg s}^{-1}$. The X-ray flare occurred approximately 170 days after the optical peak.

Based on its multi-wavelength behaviour, Wang et al. (2022) concluded that ATLAS17jrp is a robust but rare TDE discovered in the star-forming galaxy. In fact, in the entire MIRONG sample, ATLAS17jrp is the only object that displays a MIR flare and unambiguous indications of being a TDE, as evidenced by both the optical light curve and the soft X-ray emission.

2.2. The muon-track data from IceCube

IceCube released the muon-track data observed from April 2008 to July 2018¹, including 1134450 muon-track

¹ DOI: <http://doi.org/DOI:10.21234/sxvs-mt83>

events (Abbasi et al. 2021). Most events in the dataset are atmospheric muons and neutrinos from cosmic-ray air shower interactions, which are the main background for astrophysical neutrino searches. This dataset has been used for searches of point-like neutrino sources (Aartsen et al. 2020) and for catalog searches (Zhou et al. 2021). Based on the instrument response, we categorized the data into five samples corresponding different construction stages of IceCube, namely IC40, IC59, IC79, IC86-I, and IC86-II-VII. The numbers in the sample names represent the number of strings equipped with digital optical modules in the detector.

3. ANALYSIS AND RESULTS

3.1. The Time-dependent Analysis method

Based on the maximum likelihood method within the IceCube framework, we use 10-year track events to identify the time-dependent neutrino emission from ATLAS17jrp. This method models data as a two-component mixture of signal and background. The likelihood function is defined as a product over all neutrino events within the region of interest

$$\mathcal{L} = \prod_i^N \left(\frac{n_s}{N} S_i + \left(1 - \frac{n_s}{N}\right) B_i \right), \quad (1)$$

where n_s denotes the number of signal neutrinos, and N is the total number of the observed events. S_i and B_i are the signal and background probability density functions (PDFs) for the i -th event, each composed by spatial, energy, and temporal components, as follows,

$$S_i = S_i^{\text{spat}}(\vec{x}_i, \sigma_i | \vec{x}_s) S_i^{\text{ener}}(E_i | \vec{x}_s, \gamma) S_i^{\text{temp}}(t_i | t_1, t_2), \quad (2)$$

$$B_i = B_i^{\text{spat}}(\delta_i) B_i^{\text{ener}}(E_i | \delta_i) B_i^{\text{temp}}(t_i). \quad (3)$$

Here, S_i^{spat} is the signal spatial PDF, with \vec{x}_i and \vec{x}_s represent the locations of the i -th event and the source, respectively, and σ_i is the reconstructed angular uncertainty of the i -th event. The signal spatial PDF is modeled as a two-dimensional Gaussian spatial distribution (as shown in Equation (7) in Li et al. 2022). S_i^{ener} is the signal energy PDF, which describes the probability of obtaining a reconstructed energy E_i for the i -th event with an assumed spectral energy distribution (SED) (as shown in Equation (6) in Huang & Li 2022). We assume the neutrino spectrum follows a power law distribution, $dN_\nu/dE_\nu \propto E_\nu^{-\gamma}$, where E_ν is the real energy of neutrinos, and γ is the spectral index. The signal temporal PDF, S_i^{temp} , describes the temporal distribution of a set of events. We employ a box-shaped temporal PDF, where events are uniformly clustered within a defined temporal window between t_1 and t_2 , which is written as

$$S_i^{\text{temp}}(t_i | t_1, t_2) = \frac{1}{t_2 - t_1} \quad (t_1 < t_i < t_2). \quad (4)$$

The time-dependent search might reduce the background compared to the time-integrated search, thus increasing the probability of identifying the neutrino sources.

In Eq. (3), B_i^{spat} represents the background spatial PDF and B_i^{ener} is the background energy PDF, both of which are nearly uniform in right ascension, detailed descriptions can be found in Huang & Li (2022). The background temporal PDF is assumed to be constant, i.e., $B_i^{\text{temp}} = 1/T_L$, where T_L is the duration of the dataset.

In this work, we use a likelihood ratio test to compare the null and alternative hypotheses. The null hypothesis corresponds to the background-only model, denoted as $\mathcal{L}(n_s = 0)$. The alternative hypothesis involves four parameters for each source located at \vec{x}_s , which are the number of signal events n_s with $n_s \geq 0$, the spectral index γ within the range $1.0 \leq \gamma \leq 4.0$, and the start time t_1 and end time t_2 of the neutrino flare within the IceCube data sample period. The test statistic (TS) is defined as twice the log-likelihood ratio

$$\text{TS} = -2 \ln \left[\frac{\mathcal{L}(n_s = 0)}{\mathcal{L}(n_s, \gamma, t_1, t_2)} \right]. \quad (5)$$

3.2. Searching for the neutrino emission

Using the method described in Section 3.1, we search for neutrino flares during the multi-band radiation period of ATLAS17jrp, utilizing data from Wang et al. (2022). In Fig. 1, we present the multi-band light curves of ATLAS17jrp and the value of $S_i^{\text{spat}}/B_i^{\text{spat}}$ of individual IceCube events assuming ATLAS17jrp as the source. During the X-ray emission period, the time-independent weights of the neutrino events are elevated and more clustered, indicating that these neutrino events are likely associated with the X-ray emission.

We designate the start time of the neutrino flare as the peak time of the X-ray light curve, which is modified Julian day (MJD) 58169. The end time of the flare window t_2 is treated as a free parameter between MJD 58214 and MJD 58308, since *Swift*-XRT observations ceased at MJD 58214, and the end time of the 10-year IceCube data is MJD 58308. As a result, we obtain $\text{TS}_{\text{max}}=13.36$ with the best fit parameters of $\hat{n}_s=8.5$, $\hat{\gamma}=2.7$, and $\hat{t}_2=\text{MJD } 58230$, corresponding to a box-shaped time window of 61 days.

3.3. Probability by Chance

To assess the significance of the potential association between the neutrino flare identified above and the X-ray flare of ATLAS17jrp, we conduct a detailed statistical analysis. We simulate 10,000 datasets by shuffling the right ascension and the time of the events within the

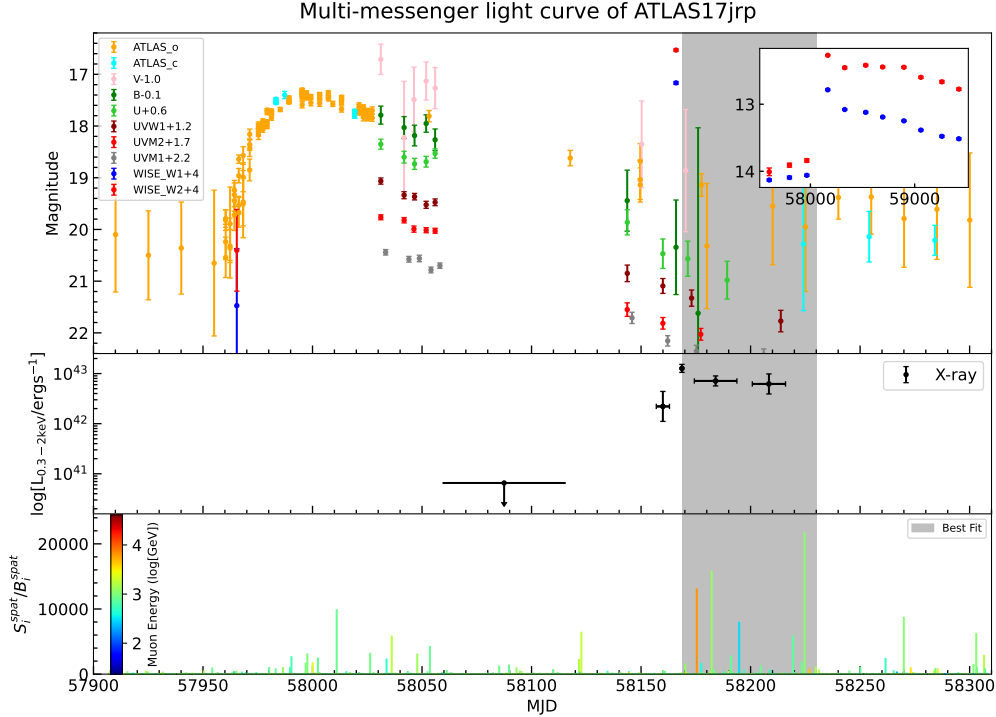


Figure 1. Top panel: Host-galaxy-subtracted light curve of ATLAS17jrp in the optical, UV, and MIR bands. The inset shows the long-term MIR light curve from WISE without host-galaxy subtraction. **Middle panel:** X-ray data of ATLAS17jrp obtained from *Swift*-XRT. The black points and arrow represent the binned X-ray light curve in the 0.3-2 keV energy range. **Bottom panel:** Time-independent weight of individual events during the multi-band radiation period of ATLAS17jrp. Each vertical line’s length represents the weight value of an event observed at a specific MJD, corresponding to the S_i^{spat}/B_i^{spat} of IceCube events. The likelihood and final significance are primarily influenced by events with high weight value. The color of each event indicates the reconstructed muon energy, from which the neutrino energy of a single event can also be inferred. The grey box shadow indicates the best-fitting neutrino flare window.

IC86-II-VII sample, to search for neutrino signals that exhibit temporal correlation with the ATLAS17jrp X-ray flare. For each set of simulations, we set t_1 at MJD 58169 and fit the parameters within the specified ranges of $n_s \geq 0$, $1.0 \leq \gamma \leq 4.0$, and t_2 ranging from MJD 58214 to MJD 58308, to calculate the maximum TS values. In this process, 17 sets of simulations yield maximum TS value greater than that obtained from the actual experimental dataset, leading to a chance probability of 1.7×10^{-3} for the association between the neutrino flare with the X-ray flare of ATLAS17jrp, corresponding to a significance of $\sim 2.9\sigma$.

4. MULTI-MESSENGER MODELING

We present the SEDs of ATLAS17jrp for the multi-messenger analysis in Fig. 2. The orange shaded area indicates the observation energy range of 0.3-10 keV for the *Swift*-XRT instrument. *Swift*-XRT detected only soft X-ray photons from ATLAS17jrp in the 0.3-2 keV range. The gray data points represent the X-ray flux at the peak time (*Swift*-XRT observation ID:

00010335009²), modeled assuming a power-law spectrum in 0.3-1 keV range. The upper limit above 1 keV is defined as the flux exceeding the background by 5σ . The light blue shaded area denotes the energy range observed by *Fermi*-LAT. No GeV counterpart was detected by *Fermi*-LAT (Ballet et al. 2024), leading to an upper limit of 1.35×10^{-12} erg cm⁻²s⁻¹ in the 0.1-100 GeV range, derived from the 14-year detection threshold map³.

Using the fitting results for n_s and γ from Section 3.2, we can calculate the corresponding $\nu_\mu + \bar{\nu}_\mu$ neutrino flux within the neutrino flare window. This calculation is based on the function of n_s as described in Eq. (6), which represents the model-predicted number of signal neutri-

² <https://www.swift.ac.uk/archive/browsedata.php?oid=00010335009&source=obs&reproc=1>

³ https://fermi.gsfc.nasa.gov/ssc/data/access/lat/14yr_catalog/detthresh_P8R3_14years_PL22.fits

nos.

$$n_s = T \times \int A_{\text{eff}}(E_\nu, \delta_i) \frac{dN_\nu}{dE_\nu}(E_\nu) dE_\nu, \quad (6)$$

where T represents the duration time of neutrino flare, A_{eff} is the effective area of the detector at declination δ_i , and the neutrino flux model is given by $dN_\nu/dE_\nu(E_\nu) = \Phi_0(E_\nu/100 \text{ TeV})^{-\gamma}$. Using the 1σ error range of $\hat{n}_s = 8.5 \pm 3.9$ and $\hat{\gamma} = 2.7 \pm 0.4$ from the fitting, we can infer the flux normalization of muon neutrino spectrum at 100 TeV, with $\Phi_{\nu_\mu + \bar{\nu}_\mu}^{100 \text{ TeV}} = 5.7_{-5.1}^{+21} \times 10^{-19} \text{ GeV}^{-1} \text{ cm}^{-2} \text{ s}^{-1}$. We multiply the muon neutrino flux by a factor of 3 to get the all-flavor neutrino flux, assuming equal flux for all flavors after oscillation.

Here, we present a lepto-hadronic modeling of the multi-wavelength and neutrino SEDs. Motivated by the temporal coincidence between the neutrino and X-ray flares, we consider the X-ray emission as target photons and investigate the multi-messenger emissions in a spherically symmetric radiation zone. The delayed soft X-ray onset in optical TDEs is usually explained by delayed accretion after circularization (Gezari et al. 2017; Liu et al. 2022), the dynamic evolution of the reprocessing layer (Thomsen et al. 2022; Guolo et al. 2024), or the interaction between winds and the surrounding cloud or torus (Mou et al. 2021). We describe the temporal behavior of the injected target photons following the X-ray light curve shown in Fig. 1. The temperature and luminosity of the target photons are derived assuming a blackbody radiation, which is consistent with the observational data. Furthermore, the radius R used in the multi-messenger modeling is consistent with the radius of the cloud/torus, approximately 10^{15} - 10^{16} cm (Markowitz et al. 2014; Mou et al. 2021). By analogy with the approach for active galactic nuclei (AGNs) (Murase et al. 2020a), an additional hard X-ray emission can be produced by the corona. We describe the hard component of the X-ray spectrum produced by the corona as a power law with an exponential cutoff, as $E^2 dN_{X,\text{cor}}/dE \propto E^{-\Gamma_{\text{cor}}} \exp(-E/E_{X,\text{cut}})$. In this expression, the spectral index and the cutoff energy can be determined by $\Gamma_{\text{cor}} \approx 0.167 \log(\lambda_{\text{Edd}})$ (Trakhtenbrot et al. 2017) and $E_{X,\text{cut}} \approx [-74 \log(\lambda_{\text{Edd}}) + 150]$ keV (Ricci et al. 2018), where $\lambda_{\text{Edd}} \approx 10L_{X,\text{cor}}/L_{\text{Edd}}$ and $L_{X,\text{cor}} = \int dE(E dN_{X,\text{cor}}/dE)$ is the corona luminosity. In this approach, the coronal X-ray spectrum can be determined solely by the luminosity $L_{X,\text{cor}}$. The coronal X-ray luminosity is estimated to be $L_{X,\text{cor}} \lesssim 5 \times 10^{42} \text{ erg s}^{-1}$ under the constraint of the observed upper limit provided by *Swift*-XRT in the 1-10 keV range.

As for the proton injection, we follow the approach of Winter & Lunardini (2023b) and Yuan & Winter (2023) by treating the injected proton luminosity as a fraction

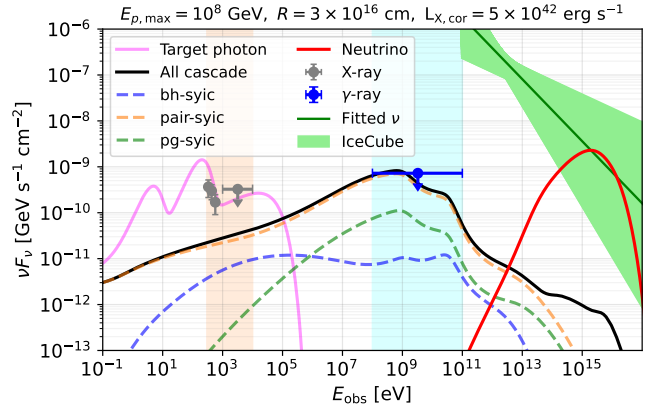


Figure 2. Multi-messenger SEDs of ATLAS17jrp. The pink, black, and red curves represent the spectra of the input target photon, the electromagnetic cascade, and all-flavor high-energy neutrino emission produced by our model, respectively. The ‘bh-syic’, ‘pair-syic’, and ‘pg-syic’ components represent the synchrotron and inverse Compton emissions from electrons and positrons produced by the Bethe-Heitler (BH), $\gamma\gamma$, and $p\gamma$ processes, respectively. The grey points represent the X-ray data at the peak time. The blue line indicate the γ -ray upper limit set by *Fermi*-LAT. The solid green line shows the best fit neutrino spectrum, with the green shaded region indicating the 68% confidence region.

of the accretion power, $L_p = \epsilon_p \dot{M}_{\text{BH}} c^2$, where $\epsilon_p = 0.2$ is a fiducial value. Since the OUV light curve follows the $t^{-5/3}$ decay, reflecting the mass fallback and accretion rate onto the supermassive black hole (SMBH), we assume that the proton injection luminosity and the accretion rate align with the OUV light curve. During the peak accreting phase, the TDE can be super-Eddington. In this case, we expect the ratio of the peak accretion rate $\dot{M}_{\text{BH}}(t_{\text{opt,peak}})$ to the Eddington accretion rate \dot{M}_{Edd} to be $\gtrsim 1$ -10 (Dai et al. 2018), where $t_{\text{opt,peak}}$ is the peak time of the OUV emission. Explicitly, we write down

$$\zeta = \frac{\dot{M}_{\text{BH}}(t_{\text{opt,peak}})}{\dot{M}_{\text{Edd}}} = \frac{\dot{M}_{\text{BH}}(t_{\text{opt,peak}})}{L_{\text{Edd}}/(\eta_{\text{rad}} c^2)} \gtrsim 1 - 10, \quad (7)$$

where $L_{\text{Edd}} \approx 1.3 \times 10^{44} (M_{\text{BH}}/10^6 M_\odot) \text{ erg s}^{-1}$ is the Eddington luminosity and the radiation efficiency $\eta_{\text{rad}} \sim 0.01 - 0.1$ (McKinney et al. 2015) represents the fraction of accreted power reprocessed to the radiation. Now, we can normalize the proton injection luminosity at $t_{\text{opt,peak}}$ via $L_p(t_{\text{opt,peak}}) = \epsilon_p (\zeta/\eta_{\text{rad}}) L_{\text{Edd}}$. In the following calculation, we adopt $\zeta/\eta_{\text{rad}} = 100$, as used by Winter & Lunardini (2023b).

We assume a power-law injection rate for the accelerated protons, i.e., $Q_p \propto E_p^{-2} \exp(-E_p/E_{p,\text{max}})$, where $E_{p,\text{max}}$ is the maximum proton energy. We normalize

the injection spectrum using L_p and the radiation zone volume $V = 4\pi R^3/3$, expressed as $\int E_p Q_p dE_p = L_p/V$. Protons can be accelerated in the compact inner jet, the accretion disk or corona, or an extended isotropic wind (Murase et al. 2020b) with a magnetic field strength of $B = 0.1\text{-}1$ G, similar to the case of AGNs. For the sake of generality, we do not specify the exact site of particle acceleration.

After protons are injected to the radiation zone, they interact with target thermal photons ($p\gamma$ process) or target protons (pp process), losing energy and producing secondary particles, which include charged/neutral pions, muons, neutrinos and electrons. Assuming the existence of the magnetic field with the strength of $B \sim 0.1$ G, neutral pions, charged leptons and the electron/positron pairs generated from $\gamma\gamma$ annihilation and BH interactions will deposit the energy into radiation, initiating the electromagnetic cascades. In this work, we use the open-source Astrophysical Multi-Messenger Modeling (AM³, Klinger et al. 2023) software to solve the time-dependent transport equations for all relevant particle species⁴.

Applying the time-dependent target photon spectra (pink curve in Fig. 2) and the proton injection rate, we evolve the system to the end time of the neutrino flare, resulting the average energy spectra of the neutrino and electromagnetic cascade over the period, shown as the red and black solid curves. In this calculation, we set parameters as $R = 3 \times 10^{16}$ cm, $B = 0.1$ G, $L_{X,\text{cor}} = 5 \times 10^{42}$ erg s⁻¹, and $E_{p,\text{max}} = 10^8$ GeV. Our results indicate that this one-zone model can explain the PeV neutrino flux without exceeding the *Fermi* γ -ray bound.

5. DISCUSSION AND CONCLUSION

In this work, we conduct a time-dependent analysis on the 10-year IceCube track data. It is noteworthy that a potential neutrino flare has been identified, exhibiting spatial and temporal association with the X-ray emission observed in the TDE ATLAS17jrp. This association has a chance probability of 0.17% ($\sim 3\sigma$ significance). If the signal is true, it is important to highlight that ATLAS17jrp is the second TDE that associated with neutrinos, following the first one AT2019dsg. In contrast, AT2019fdr (Frederick et al. 2021; Pitik et al. 2022) and AT2019aalc (van Velzen et al. 2024) are considered as AGN flares, while the two events from Jiang et al. (2023) that lack optical and X-ray flares are classified as obscured TDE candidates.

In this context, we calculate the neutrino and electromagnetic cascade emissions from the $p\gamma$ processes, since the pp interactions are typically subdominant in isotropic TDE winds (Yuan & Winter 2023). We assume X-rays as the target photons for the $p\gamma$ process. The delayed IR photons may also contribute to the neutrino production, but they are negligible in our scenario due to two key factors. First, the delayed IR may be generated by re-emission processes in the dust torus after being heated by OUV and X-ray radiation, resulting in a lower photon density due to isotropization over a much larger volume with radius $R_{\text{dust}} \gg R$. Second, Yuan & Winter (2023) indicated that 0.1 eV IR photons primarily contribute to neutrino production above 10 PeV.

Under specific parameter assumptions, we present the corresponding electromagnetic cascade and neutrino spectra in Fig. 2. For ATLAS17jrp, our model explains the tentative PeV neutrino flux without violating the γ -ray upper limit observed by *Fermi*-LAT. The 1-10 TeV neutrinos can be explained in two ways. One explanation needs a high luminosity of the injected protons, which requires more efficient proton acceleration sites and an additional absorption mechanism to reach the neutrino luminosity of $L_\nu \sim 8 \times 10^{45}$ erg s⁻¹ while depleting the cascade γ -rays. The upper limit from *Swift* in the 1-10 keV is crucial, as it constrains the target photon density, which is directly linked to the efficiency of neutrino production and the absorption of γ -ray photons. The delayed X-rays may come from the wind-cloud/torus interaction, corresponding to radiation at a radius of $R \sim 10^{15}\text{-}10^{16}$ cm, which can further limit the $\gamma\gamma$ optical depth. The other explanation requires target photons above MeV to contribute to the 1-10 TeV neutrinos, but this source lacks observations above MeV. Prospective MeV telescopes may provide more information on MeV target photons for similar cases in the future.

Future precise measurement of neutrino energy spectra and correlations from multi-wavelength observations will enhance our understanding of radiation models. These efforts will be crucial for uncovering the underlying mechanisms of high-energy astrophysical processes and origins of neutrinos. The neutrino telescopes currently under development and those to come, such as the Cubic Kilometre Neutrino Telescope (KM3NeT) (Adrian-Martinez et al. 2016), IceCube-Gen2 (Aartsen et al. 2021; Clark 2021), the Tropical Deep-sea Neutrino Telescope (TRIDENT) (Ye et al. 2023), and the High-energy Underwater Neutrino Telescope (HUNT) (Huang et al. 2023) could detect more high energy neutrino flares. Combined with multi-messenger observations, it

⁴ A detailed description of the particle energy loss and diffusion terms can be found in Yuan & Winter (2023)

will enable the identification of high-energy astrophysical neutrino origins and further advance time-domain multi-messenger astronomy.

ACKNOWLEDGMENTS

H.N.He is supported by Project for Young Scientists in Basic Research of Chinese Academy of Sciences (No. YSBR-061), and by NSFC under the grants

No.12173091, No.12333006, and No.12321003, and the Strategic Priority Research Program of the Chinese Academy of Sciences No.XDB0550400. Y.Wang is supported by the Jiangsu Funding Program for Excellent Postdoctoral Talent (grant No.2024ZB110) and the Postdoctoral Fellowship Program of CPSF under Grant Number GZC20241916.

REFERENCES

- Aartsen, M. G., et al. 2013, *Science*, 342, 1242856, doi: [10.1126/science.1242856](https://doi.org/10.1126/science.1242856)
- . 2014, *Phys. Rev. Lett.*, 113, 101101, doi: [10.1103/PhysRevLett.113.101101](https://doi.org/10.1103/PhysRevLett.113.101101)
- Aartsen, M. G., Ackermann, M., Adams, J., et al. 2020, *Phys. Rev. Lett.*, 124, 051103, doi: [10.1103/PhysRevLett.124.051103](https://doi.org/10.1103/PhysRevLett.124.051103)
- Aartsen, M. G., et al. 2021, *J. Phys. G*, 48, 060501, doi: [10.1088/1361-6471/abbd48](https://doi.org/10.1088/1361-6471/abbd48)
- Abbasi, R., et al. 2021, doi: [10.21234/CPKQ-K003](https://doi.org/10.21234/CPKQ-K003)
- . 2023, *Astrophys. J. Suppl.*, 269, 25, doi: [10.3847/1538-4365/acfa95](https://doi.org/10.3847/1538-4365/acfa95)
- Adrian-Martinez, S., et al. 2016, *J. Phys. G*, 43, 084001, doi: [10.1088/0954-3899/43/8/084001](https://doi.org/10.1088/0954-3899/43/8/084001)
- Ahlers, M., & Halzen, F. 2017, *Progress of Theoretical and Experimental Physics*, 2017, 12A105, doi: [10.1093/ptep/ptx021](https://doi.org/10.1093/ptep/ptx021)
- Ballet, J., Bruel, P., Burnett, T. H., Lott, B., & collaboration, T. F.-L. 2024, Fermi Large Area Telescope Fourth Source Catalog Data Release 4 (4FGL-DR4). <https://arxiv.org/abs/2307.12546>
- Bellm, E. C., Kulkarni, S. R., Graham, M. J., et al. 2019, *PASP*, 131, 018002, doi: [10.1088/1538-3873/aaecbe](https://doi.org/10.1088/1538-3873/aaecbe)
- Cannizzo, J. K., Lee, H. M., & Goodman, J. 1990, *ApJ*, 351, 38, doi: [10.1086/168442](https://doi.org/10.1086/168442)
- Clark, B. 2021, *JINST*, 16, C10007, doi: [10.1088/1748-0221/16/10/C10007](https://doi.org/10.1088/1748-0221/16/10/C10007)
- Dai, L., & Fang, K. 2017, *MNRAS*, 469, 1354, doi: [10.1093/mnras/stx863](https://doi.org/10.1093/mnras/stx863)
- Dai, L., McKinney, J. C., Roth, N., Ramirez-Ruiz, E., & Miller, M. C. 2018, *ASTROPHYSICAL JOURNAL LETTERS*, 859, doi: [10.3847/2041-8213/aab429](https://doi.org/10.3847/2041-8213/aab429)
- Dai, L., McKinney, J. C., Roth, N., Ramirez-Ruiz, E., & Miller, M. C. 2018, *ApJL*, 859, L20, doi: [10.3847/2041-8213/aab429](https://doi.org/10.3847/2041-8213/aab429)
- Evans, C. R., & Kochanek, C. S. 1989, *ApJL*, 346, L13, doi: [10.1086/185567](https://doi.org/10.1086/185567)
- Fang, K., Metzger, B. D., Vurm, I., Aydi, E., & Chomiuk, L. 2020, *ApJ*, 904, 4, doi: [10.3847/1538-4357/abbc6e](https://doi.org/10.3847/1538-4357/abbc6e)
- Frederick, S., Gezari, S., Graham, M. J., et al. 2021, *The Astrophysical Journal*, 920, 56, doi: [10.3847/1538-4357/ac110f](https://doi.org/10.3847/1538-4357/ac110f)
- Gezari, S., Cenko, S. B., & Arcavi, I. 2017, *Astrophys. J. Lett.*, 851, L47, doi: [10.3847/2041-8213/aaa0c2](https://doi.org/10.3847/2041-8213/aaa0c2)
- Guépin, C., Kotera, K., & Oikonomou, F. 2022, *Nature Rev. Phys.*, 4, 697, doi: [10.1038/s42254-022-00504-9](https://doi.org/10.1038/s42254-022-00504-9)
- Guolo, M., Gezari, S., Yao, Y., et al. 2024, A systematic analysis of the X-ray emission in optically selected tidal disruption events: observational evidence for the unification of the optically and X-ray selected populations. <https://arxiv.org/abs/2308.13019>
- Hayasaki, K., & Yamazaki, R. 2019, *ApJ*, 886, 114, doi: [10.3847/1538-4357/ab44ca](https://doi.org/10.3847/1538-4357/ab44ca)
- Huang, T.-Q., Cao, Z., Chen, M., et al. 2023, *PoS, ICRC2023*, 1080, doi: [10.22323/1.444.1080](https://doi.org/10.22323/1.444.1080)
- Huang, T.-Q., & Li, Z. 2022, *Monthly Notices of the Royal Astronomical Society*, 514, 852, doi: [10.1093/mnras/stac1350](https://doi.org/10.1093/mnras/stac1350)
- Jiang, N., Wang, T., Hu, X., et al. 2021a, *Astrophys. J.*, 911, 31, doi: [10.3847/1538-4357/abe772](https://doi.org/10.3847/1538-4357/abe772)
- Jiang, N., Zhou, Z., Zhu, J., Wang, Y., & Wang, T. 2023, *Astrophys. J. Lett.*, 953, L12, doi: [10.3847/2041-8213/acebe3](https://doi.org/10.3847/2041-8213/acebe3)
- Jiang, N., Wang, T., Dou, L., et al. 2021b, *ASTROPHYSICAL JOURNAL SUPPLEMENT SERIES*, 252, doi: [10.3847/1538-4365/abd1dc](https://doi.org/10.3847/1538-4365/abd1dc)
- Klinger, M., Rudolph, A., Rodrigues, X., et al. 2023, arXiv e-prints, arXiv:2312.13371, doi: [10.48550/arXiv.2312.13371](https://doi.org/10.48550/arXiv.2312.13371)
- Li, R.-L., Zhu, B.-Y., & Liang, Y.-F. 2022, *Phys. Rev. D*, 106, 083024, doi: [10.1103/PhysRevD.106.083024](https://doi.org/10.1103/PhysRevD.106.083024)
- Liu, X.-L., Dou, L.-M., Chen, J.-H., & Shen, R.-F. 2022, *The Astrophysical Journal*, 925, 67, doi: [10.3847/1538-4357/ac33a9](https://doi.org/10.3847/1538-4357/ac33a9)
- Lunardini, C., & Winter, W. 2017, *PhRvD*, 95, 123001, doi: [10.1103/PhysRevD.95.123001](https://doi.org/10.1103/PhysRevD.95.123001)
- Markowitz, A. G., Krumpe, M., & Nikutta, R. 2014, *MNRAS*, 439, 1403, doi: [10.1093/mnras/stt2492](https://doi.org/10.1093/mnras/stt2492)

- McKinney, J. C., Dai, L., & Avara, M. J. 2015, *MNRAS*, 454, L6, doi: [10.1093/mnras/slv115](https://doi.org/10.1093/mnras/slv115)
- Mou, G., Dou, L., Jiang, N., et al. 2021, *ApJ*, 908, 197, doi: [10.3847/1538-4357/abd475](https://doi.org/10.3847/1538-4357/abd475)
- Murase, K., & Bartos, I. 2019, *Ann. Rev. Nucl. Part. Sci.*, 69, 477, doi: [10.1146/annurev-nucl-101918-023510](https://doi.org/10.1146/annurev-nucl-101918-023510)
- Murase, K., Kimura, S. S., & Mészáros, P. 2020a, *PhRvL*, 125, 011101, doi: [10.1103/PhysRevLett.125.011101](https://doi.org/10.1103/PhysRevLett.125.011101)
- Murase, K., Kimura, S. S., Zhang, B. T., Oikonomou, F., & Petropoulou, M. 2020b, *ApJ*, 902, 108, doi: [10.3847/1538-4357/abb3c0](https://doi.org/10.3847/1538-4357/abb3c0)
- Onori, F., Cannizzaro, G., Jonker, P. G., et al. 2022, *MONTHLY NOTICES OF THE ROYAL ASTRONOMICAL SOCIETY*, 517, 76, doi: [10.1093/mnras/stac2673](https://doi.org/10.1093/mnras/stac2673)
- Phinney, E. S. 1989, in *The Center of the Galaxy*, ed. M. Morris, Vol. 136, 543
- Pitik, T., Tamborra, I., Angus, C. R., & Auchettl, K. 2022, *Astrophys. J.*, 929, 163, doi: [10.3847/1538-4357/ac5ab1](https://doi.org/10.3847/1538-4357/ac5ab1)
- Rees, M. J. 1988, *Nature*, 333, 523, doi: [10.1038/333523a0](https://doi.org/10.1038/333523a0)
- Reusch, S., et al. 2022a, *Phys. Rev. Lett.*, 128, 221101, doi: [10.1103/PhysRevLett.128.221101](https://doi.org/10.1103/PhysRevLett.128.221101)
- . 2022b, *Phys. Rev. Lett.*, 128, 221101, doi: [10.1103/PhysRevLett.128.221101](https://doi.org/10.1103/PhysRevLett.128.221101)
- Ricci, C., Ho, L. C., Fabian, A. C., et al. 2018, *MNRAS*, 480, 1819, doi: [10.1093/mnras/sty1879](https://doi.org/10.1093/mnras/sty1879)
- Stein, R., Velzen, S. v., Kowalski, M., et al. 2021, *Nature Astronomy*, 5, 510–518, doi: [10.1038/s41550-020-01295-8](https://doi.org/10.1038/s41550-020-01295-8)
- Thomsen, L. L., Kwan, T. M., Dai, L., Wu, S. C., & Ramirez-Ruiz, E. 2022, *Astrophys. J. Lett.*, 937, L28, doi: [10.3847/2041-8213/ac911f](https://doi.org/10.3847/2041-8213/ac911f)
- Tonry, J. L., Denneau, L., Heinze, A. N., et al. 2018, *PUBLICATIONS OF THE ASTRONOMICAL SOCIETY OF THE PACIFIC*, 130, doi: [10.1088/1538-3873/aabadf](https://doi.org/10.1088/1538-3873/aabadf)
- Trakhtenbrot, B., Ricci, C., Koss, M. J., et al. 2017, *MNRAS*, 470, 800, doi: [10.1093/mnras/stx1117](https://doi.org/10.1093/mnras/stx1117)
- van Velzen, S., et al. 2024, *Mon. Not. Roy. Astron. Soc.*, 529, 2559, doi: [10.1093/mnras/stae610](https://doi.org/10.1093/mnras/stae610)
- Wang, X.-Y., & Liu, R.-Y. 2016, *PhRvD*, 93, 083005, doi: [10.1103/PhysRevD.93.083005](https://doi.org/10.1103/PhysRevD.93.083005)
- Wang, X.-Y., Liu, R.-Y., Dai, Z.-G., & Cheng, K. S. 2011, *PhRvD*, 84, 081301, doi: [10.1103/PhysRevD.84.081301](https://doi.org/10.1103/PhysRevD.84.081301)
- Wang, Y., Jiang, N., Wang, T., et al. 2022, *ASTROPHYSICAL JOURNAL LETTERS*, 930, doi: [10.3847/2041-8213/ac6670](https://doi.org/10.3847/2041-8213/ac6670)
- Winter, W., & Lunardini, C. 2023a, *ASTROPHYSICAL JOURNAL*, 948, doi: [10.3847/1538-4357/acbe9e](https://doi.org/10.3847/1538-4357/acbe9e)
- . 2023b, *The Astrophysical Journal*, 948, 42, doi: [10.3847/1538-4357/acbe9e](https://doi.org/10.3847/1538-4357/acbe9e)
- Wright, E. L., Eisenhardt, P. R. M., Mainzer, A. K., et al. 2010, *AJ*, 140, 1868, doi: [10.1088/0004-6256/140/6/1868](https://doi.org/10.1088/0004-6256/140/6/1868)
- Ye, Z. P., Hu, F., Tian, W., et al. 2023, *Nature Astronomy*, 7, 1497, doi: [10.1038/s41550-023-02087-6](https://doi.org/10.1038/s41550-023-02087-6)
- Yuan, C., & Winter, W. 2023, *ApJ*, 956, 30, doi: [10.3847/1538-4357/acf615](https://doi.org/10.3847/1538-4357/acf615)
- Yuan, C., Winter, W., & Lunardini, C. 2024a, *The Astrophysical Journal*, 969, 136, doi: [10.3847/1538-4357/ad50a9](https://doi.org/10.3847/1538-4357/ad50a9)
- Yuan, C., Zhang, B. T., Winter, W., & Murase, K. 2024b, *Structured Jet Model for Multiwavelength Observations of the Jetted Tidal Disruption Event AT 2022cmc*. <https://arxiv.org/abs/2406.11513>
- Zheng, J.-H., Liu, R.-Y., & Wang, X.-Y. 2023, *ASTROPHYSICAL JOURNAL*, 954, doi: [10.3847/1538-4357/ace71c](https://doi.org/10.3847/1538-4357/ace71c)
- Zhou, B., Kamionkowski, M., & Liang, Y.-f. 2021, *Phys. Rev. D*, 103, 123018, doi: [10.1103/PhysRevD.103.123018](https://doi.org/10.1103/PhysRevD.103.123018)